Report of the CCRI(II) supplementary international comparison of measurement of activity per unit mass of Cs-134 and Cs-137 in wheat flour (CCRI(II)-S13)

Akira Yunoki[1)], Tsutomu Miura[1)], Rio Furukawa[1)], Franz Josef Maringer[2)], Hannah Wiedner[2)], Virginia Peyres Medina[3)], Aldo Fazio[4)], Andrea Petrucci[4)], Aurelian Luca[5)], Mihail-Razvan Ioan[5)], Andrei Antohe[5)], Maria Sahagia[5)], Catalina Cimpeanu[5)], Boštjan Črnič[6)], Denis Glavič-Cindro[6)], Marijan Nečemer[6)], Toni Petrovič[6)], Branko Vodenik[6)], Benjamin Zorko[6)], Guillaume Lutter[7)], Gerd Marissens[7)], J. M. Lee[8)], K. B. Lee[8)], M. K. Lee[8)], D. H. Heo[8)], S. H. Hwang[8)], Jerome La Rosa[9)], Svetlana Nour[9)], Milton van Rooy[10)], Joline Lubbe[10)], Martin van Staden[10)], Andrej Javornik[11)], Michaela Zalesakova[11)], Jarmila Ometakova[11)], Emin Yeltepe[12)], Mayumi Hachinohe[13)] and Shioka Hamamatsu [13)]

[1)] National Metrology Institute of Japan, National Institute of Advanced Industrial Science and Technology, 1-1-1 Umezono, Tsukuba, Ibaraki 305-8568, Japan.
[2)] Bundesamt für Eich- und Vermessungswesen, Arltgasse 35, 1160 Wien, Austria.
[3)] Centro de Investigaciones Energéticas, Medioambientales y Tecnológicas, Avda Complutense 40, 28040 Madrid, Spain.
[4)] Italian National Agency for New Technologies, Energy and Sustainable Economic Development, National Institute of Ionizing Radiation Metrology, C.R. Casaccia - Via Anguillarese, 301, I-00123 Rome, Italy.
[5)] Horia Hulubei National Institute for Research and Development in Physics and Nuclear Engineering / Radionuclide Metrology Laboratory, 30 Reactorului street, Magurele, Ilfov county, RO 077125, Romania.
[6)] Department of low and medium energy physics, Jožef Stefan Institute, Jamova cesta 39, SI-1000 Ljubljana, Slovenia.
[7)] European Commission, Joint Research Centre in Geel, Retieseweg 111, 2440 Geel, Belgium.
[8)] Korea Research Institue of Standards and Science, 267 Gajeong-Ro, Yuseong-Gu, Daejeon 34113, Republic of Korea.
[9)] National Institute of Standards and Technology, 100 Bureau Drive, MS 8462, Gaitherburg, MD 20899-8462, USA.
[10)] National Metrology Institute of South Africa, 15 Lower Hope Road, CSIR Campus, Rosebank, Cape Town, 7700, South Africa.
[11)] Slovak Insitute of Metrology, Karloveská 63, 842 55 Bratislava, Slovakia.
[12)] Turkish Energy, Nuclear and Mineral Research Agency - Nuclear Energy Research Institute, Saray M. Atom CD. NO: 27, Kazan Ankara, Turkey.
[13)] National Agriculture and Food Research Organization, 3-1-1 Kannondai, Tsukuba, Ibaraki 305-8517, Japan.

Abstract

A supplementary international comparison of measurement of activity per unit mass of Cs-134 and Cs-137 in wheat flour (CCRI(II)-S13) was carried out by CCRI in 2018. The matrix of the sample was wheat harvested in 2011 after the Fukushima Daiichi Nuclear Power Plant accident. No spiking was applied to the sample. Twelve institutes reported their results. Averages of the reported results and the associated uncertainties were obtained using the power-moderated mean. This report describes the supplementary comparison reference value, the degrees of equivalence of the results, the procedures of this comparison, and the sample preparation and measurements by the participants. Successful participation in this comparison by a laboratory may provide evidential support for Calibration and Measurement Capability (CMC) claims for Cs-134 and Cs-137 measured using the laboratory's method(s) used in the comparison or methods calibrated by those used for the comparison.

1. Introduction

After the accident of Fukushima Daiichi Nuclear Power Plant, many measurement institutes began to measure the radioactivity of various foods. Consequently, the importance of reliable measurements of radionuclides in food increased significantly. The National Metrology Institute of Japan, National Institute of Advanced Industrial Science and Technology (NMIJ/AIST) and Institute of Food Research, the National Agriculture and Food Research Organization (NARO) of Japan developed a certified reference material (CRM) of brown rice grain containing Cs-134 and Cs-137 (NMIJ CRM 7541-a/b) to provide a tool to validate the measurement methods [1-3]. The NMIJ/AIST and NARO held several domestic comparisons of activity measurements using the rice samples [4]. Furthermore, the NMIJ/AIST conducted the APMP regional international comparison of brown rice (APMP.RI(II)-S3.Cs-134.Cs-137) [5]. However, in many other countries, the consumption of wheat was larger. Therefore, to satisfy the potential requirement of wheat sample measurements, NMIJ/AIST proposed an international supplementary comparison of measurement of activity per unit mass of Cs-134 and Cs-137 in wheat flour at the CCRI(II) meeting of 2015. The proposal was approved and NMIJ/AIST was assigned as a pilot laboratory. A sample was prepared by NARO using wheat harvested in 2011 after the Fukushima Daiichi Nuclear Power Plant accident that contained distributed Cs-134 and Cs-137, of which the activities were approximately the same. NARO milled and homogenized the wheat grain. In 2018, each participant received three packages of sample whose amount (wet, net mass) was controlled to be (81.00±0.02) g per package. Twelve institutes reported their results. In this report, the supplementary comparison reference value (SCRV) and the degrees of equivalence (DoE) of the results are reported. The procedures for this comparison, the sample preparation and measurements by the participants are also described. Successful participation in this comparison by a laboratory may provide evidential support for Calibration and Measurement Capability (CMC) claims for Cs-134 and Cs-137 measured using the laboratory's method(s) used in the comparison or methods calibrated by those used for the comparison.

2. Technical protocol

2.1 Measurement

Each participant received three vessels containing wheat flour samples and were asked to report activities of Cs-134 and Cs-137 per dry mass [in Bq kg^{-1}] in the sample. Uncertainty estimation was performed according to the Guide to the expression of Uncertainty in Measurement (GUM) [6]. The reference date of the measurement was 1 March 2018 UTC 0:00:00.

2.2 Time schedule

The samples were shipped to the participants in April-June 2018. The deadline for reporting was 15 November 2018. The NMIJ/AIST prepared a draft A report at the end of March 2022. During its circulation among the participants, the ENEA-INMRI found that they reported an incorrect result of moisture content, and the IJS found that they calculated activity per unit mass by dividing the activity by wet mass. The NMIJ/AIST revised the Draft A report reflecting these changes and re-circulated it with a summary of the changes in December of 2022. All of the participants agreed to the changes by 20 January 2023. Then, the NMIJ/AIST submitted it to the CCRI/KCWG(II) in accordance with Appendix B of CIPM MRA-G-11 “Measurement comparisons in the CIPM MRA – Guidelines for organizing, participating and reporting”.

2.3 Evaluation of the comparison results

The result of each participant was evaluated by the degree of equivalence (DoE) with the SCRV. The SCRV was obtained by using the power-moderated mean (PMM) [7].

3. Participants

Table 1 lists the acronyms of participants, their full names, countries and Regional Metrological Organizations (RMO).

Table 1. Acronyms, full names, countries and RMOs of participants.

Acronym	Full name	Country	RMO
BEV	Bundesamt für Eich- und Vermessungswesen	Austria	EURAMET
CIEMAT	Centro de Investigaciones Energéticas, Medioambientales y Tecnológicas	Spain	EURAMET
ENEA-INMRI	Italian National Agency for New Technologies, Energy and Sustainable Economic Development, National Institute of Ionizing Radiation Metrology	Italy	EURAMET
IFIN-HH	Horia Hulubei National Institute for Research and Development in Physics and Nuclear Engineering/Radionuclide Metrology Laboratory	Romania	EURAMET
IJS	Jožef Stefan Institute	Slovenia	EURAMET
JRC-Geel	European Commission, Joint Research Centre	EU	EURAMET
KRISS	Korea Research Institute of Standards and Science	Korea	APMP

Table 1. Acronyms, full names, countries and RMOs of participants (continued).

Acronym	Full name	Country	RMO
NIST	National Institute of Standards and Technology	United States of America	SIM
NMISA	National Metrology Institute of South Africa	South Africa	AFRIMET
SMU	Slovak Institute of Metrology	Slovakia	EURAMET
TENMAK-NÜKEN	Turkish Energy, Nuclear and Mineral Research Agency-Nuclear Energy Research Institute	Turkey	EURAMET
NMIJ/AIST	National Metrology Institute of Japan, National Institute of Advanced Industrial Science and Technology	Japan	APMP

4. Preliminary measurements

Some participants reported results of preliminary measurements, which are listed in Table 2.

Table 2. Results of preliminary measurements.

Institute	Measurement method	Result with standard uncertainty	
		Cs-134	Cs-137
BEV	In the BEV's standard sample container (⌀64 × 11 mm).	(9.5±0.5) Bq kg^{-1}	(99±4) Bq kg^{-1}
CIEMAT	In the distributed container.	0.774 Bq	6.53 Bq
ENEA-INMRI	In the INMRI reference container, measured count rate per unit mass (wet).	Not measured.	#12: 0.0136 s^{-1} kg^{-1} #13: 0.0141 s^{-1} kg^{-1} #16: 0.0136 s^{-1} kg^{-1}
JRC-Geel	In the distributed container. Assumed moisture content 10 %.	#4: (10.7±1.0) Bq kg^{-1} #5: (10.6±1.0) Bq kg^{-1} #7: (10.5±1.0) Bq kg^{-1}	#4: (94.3±5.0) Bq kg^{-1} #5: (93.0±5.0) Bq kg^{-1} #7: (93.8±5.0) Bq kg^{-1}
NIST	Measured activity of 70 g sample (1 Oct. 2018).	0.57 Bq	5.7 Bq
SMU	In the distributed container.	#25: 0.74 Bq #26: 0.76 Bq #27: 0.75 Bq	#25: 6.77 Bq #26: 6.70 Bq #27: 6.79 Bq
TENMAK-NÜKEN	In the distributed container.	#45: (12.2±1.0) Bq kg^{-1} #47: (11.0±0.9) Bq kg^{-1} #48: (13.3±1.1) Bq kg^{-1}	#45: (92.6±6.0) Bq kg^{-1} #47: (90.0±6.0) Bq kg^{-1} #48: (93.3±6.1) Bq kg^{-1}

5. Sample preparation

NARO prepared raw sample material using naturally contaminated wheat flour. The wheat (*Triticum aestivum* L) was harvested three months after the Fukushima Daiichi Nuclear Power Plant accident. It was milled using a laboratory test mill (Buhler Inc. MLU-202) to obtain eight fractions: 1B, 2B, 3B, 1M, 2M, 3M, bran, and short. A mixture of 1B, 2B, 1M and 2M was used for the samples. The

median diameter of the flour particles, measured by laser diffraction, was 82.6 μm [8]. The samples were not spiked with either Cs-134 or Cs-137. The homogenized wheat flour was packaged in approximately 100 cm^3 polypropylene vessels [9]. The amount (wet, net mass) was controlled to be (81.00±0.02) g per package. The bulk density of the wheat flour was approximately 0.95 g cm^{-3}. The top of each package was sealed with a thin film of paraffin. An acrylic plate and a polystyrene foam plate were inserted between the thin film of paraffin and the cap of the vessel to avoid movement of the wheat flour. The height of the sample was 48 mm from the bottom. The samples were sterilized by gamma-irradiation of 27 kGy -29 kGy to facilitate transport across national borders. Each participant received three packages of the sample. Table 3 lists the numbers of the samples distributed to the participants.

Table 3. Number of samples distributed to participants.

NMI	Sample number
BEV	1, 2, 3
CIEMAT	40, 41, 43
ENEA-INMRI	12, 13, 16
IFIN-HH	22, 23, 24
IJS	37, 38, 39
JRC-Geel	4, 5, 7
KRISS	17, 19, 20
NIST	30, 32, 33
NMISA	46, 49, 50
SMU	25, 26, 27
TENMAK-NÜKEN	45, 47, 48
NMIJ/AIST	57, 58, 59

NMIJ/AIST measured the activities of the samples using HPGe detectors (ORTEC GEM 130-108). The sample vessel was set at the center of the end cap of the detector and the position was determined using a circular jig. The photopeak at 796 keV was used for Cs-134 and that at 662 keV was used for Cs-137. Peak counting efficiencies (count per photon, s^{-1} Bq^{-1}) were calibrated using standard solutions of Cs-134 and Cs-137 contained in the same type of vessel as that used for the sample. The difference in efficiency due to the difference of sample height and self-attenuation was adjusted using EGS5. To evaluate the homogeneity of the samples, 20 randomly selected samples were measured twice each. Standard uncertainties associated with the variety between bottles, s_{bb} and u_{bb} [10], determined by using Equations (1) and (2), were analyzed by analysis of variance (ANOVA) testing, and the results are listed in Table 4.

$$s_{bb} = \sqrt{\frac{MS_{among} - MS_{within}}{n}}, \quad (1)$$

$$u_{bb} = \sqrt{\frac{MS_{within}}{n}} \times \sqrt[4]{\frac{2}{v_{MS_{within}}}}, \quad (2)$$

where MS_{among} is the between-bottle mean square, MS_{within} is the within-bottle mean square, n is the number of repeated measurements, and $v_{MSwithin}$ is the degrees of freedom of MS_{within}.

Table 4. Variance between bottles, s_{bb} and u_{bb} [10].

Variance between bottles	Cs-134	Cs-137
s_{bb}	1.45 %	0.69 %
u_{bb}	0.95 %	0.27 %

6. Sample treatment by the participants

BEV prepared two samples by filling representative moist samples into measurement containers (64 mm diameter, 11 mm height).

CIEMAT, IFIN-HH, KRISS and NMIJ/AIST used the distributed samples as received.

ENEA-INMRI used its polyethylene reference geometry container and filled sample to a total amount of 87.37324 g (wet mass), which corresponded to a volume of 100.0 cm^3.

IJS placed the sample material into 90 mm diameter plastic containers and pressed to obtain evenly distributed sample with a well-defined thickness. The thickness of the sample was measured at 5 points; on this basis, the average thickness, and the uncertainty of the sample thickness was calculated.

JRC-Geel transferred a part of each sample to a radon tight Teflon container. The new samples contained respectively (51.5732±0.0001) g, (54.4885±0.0001) g and (53.7213±0.0001) g of sample material.

NIST transferred approximately 70 g of undried sample to a tared plastic sample jar (83 mm internal diameter, 40 mm height, approximately 1.4 mm wall thickness) with a screw-cap lid and approximately leveled at 100 cm^3. All of the three wheat flour sample densities were measured to be about 0.7 g cm^{-3}.

NMISA prepared three samples by filling into 75 cm^3 plastic pill boxes to obtain 33.799 g, 31.967 g and 33.894 g samples in wet mass.

SMU transferred the samples into 450 cm^3 Marinelli beakers (232.85 g), and lightly pressed the sample to a density of 0.8715 g cm^{-3} (calculated from the volume of 267.17 cm^3).

TENMAK-NÜKEN transferred the samples to 6 cm×5 cm polypropylene containers commonly used in TENMAK-NÜKEN.

7. Peak count efficiency calibration

BEV calculated peak count efficiency using MC based via LabSOCS (Canberra Genie 2000) software.

CIEMAT calibrated counting efficiencies by Monte Carlo simulation (PENELOPE) modeling the source and using a detector model validated with liquid sources of Cs-134 and Cs-137 in the same geometry (The sources were measured in two geometries, at 0.5 cm and 3 cm of the detector window).

ENEA-INMRI obtained full energy peak (FEP) counting efficiency for Cs-134 and Cs-137 from the efficiency curve of the calibrated HPGe detector, traceable to the ENEA-INMRI National Activity Standard. A log/log linear fit was used in the energy range higher than 220 keV.

IFIN-HH calibrated the efficiency using a cylindrical volume radioactive standard source in a water equivalent matrix, produced by IFIN-HH/LMR, which contained a mixture of radionuclides: Am-241, Ba-133, Eu-152, Cs-137 and Co-60. Geometry corrections and true coincidence summing corrections were applied to the experimental data using the efficiency transfer and the coincidence summing correction tools of the GESPECOR ver. 4.2 software (CID Media GmbH, Germany).

IJS determined the efficiency with an in-house-developed characterization procedure. Certified point sources of several gamma-ray emitters were placed on a grid of points above the detector cap to determine the response of the detector at each point for all selected energies. An efficiency calibration curve was then constructed for each point. The efficiency for volume sources was calculated numerically by integrating the registered spatial response of the detector over the volume of the sample, taking into account self-attenuation in the sample material. The efficiency is checked regularly on biannual basis with certified multigamma aqueous solution provided by Eckert & Ziegler. The solution contains following radionuclides: Am-241, Cd-109, Co-57, Co-60, Ce-139, Cs-137, Hg-203, Sn-113, Sr-85 and Y-88.

JRC-Geel calculated the FEP efficiencies using the efficiency transfer method by first establishing an experimental calibration curve and then calculating correction factors for differences between the calibration sample and the wheat samples using Monte Carlo simulations. The experimental FEP efficiencies were given by a reference source produced by CMI (Czech Republic) containing the following radionuclides: Pb-210, Co-60, Cs-137, Am-241, Ba-133, Cd-109, Ce-139, Co-57, Cr-51, Sn-113, Sr-85 and Y-88. Due to technical constraints, the experimental FEP efficiencies were measured for the "Ge-3" detector using a liquid solution from the NPL proficiency test 2012, which contains Ba-133, Cs-134, Cs-137 and Eu-152. The reference sources were placed at the same position as the samples. The density, matrix, geometry and coincidence summing were corrected using in-house developed code based on the EGSnrc Monte Carlo framework [11].

KRISS used two certified calibration sources. Both sources were contained in containers that were distributed by NMIJ/AIST. One of the sources (CRM No. 181U890STD) contained Am-241, Cd-109, Co-57, Ce-139, Cr-51, Sn-133, Sr-85, Cs-137, Co-60 and Y-88. The other source (CRM No. 18MIX2U890) contained Cs-137 and Cs-134. Each nuclide had been certified using the gamma reference chamber at KRISS. The peak efficiency (s^{-1} Bq^{-1}) of Cs-137 and Cs-134 were estimated from a peak-to-peak activity comparison.

NIST prepared 80 cm^3, 90 cm^3 and 100 cm^3 ethanol solutions (referred to as comparator standards) spiked with known activities of Cs-134 and Cs-137 in the sample jars from accurate dilutions of

SRM 4233D (Cs-137) and NIST-calibrated Cs-134 solutions. The gamma ray photopeak counting efficiencies, (net photopeak rate, s^{-1}) / (nuclide activity, Bq), were determined as a function of sample volume. The counting efficiency for the 605 keV and 796 keV γ-emissions were used for Cs-134, and that for the 662 keV γ-emission was used for Cs-137.

NMISA obtained the peak count efficiency and its associated uncertainty using LabSOCS. The pill box geometry was modeled in LabSOCS, and efficiency curves were determined for each counting sample using the matrix of wheat flour [12].

SMU obtained the peak count efficiency using efficiency transfer from the point source to the Marinelli beaker geometry corrected for different volumes using ANGLE code. SMU applied further correction using calibrated water samples with the same volume in the Marinelli beaker.

TENMAK-NÜKEN used dedicated software (ANGLE and EFFTRAN) and obtained the peak count efficiency using efficiency transfer from a reference material that contained Cs-134 and Cs-137 with a similar chemical composition and density as the wheat flour. The detector was also characterized with EGSnrc Monte-Carlo simulation code. The differences were less than 1.5 % between the simulation and the experimental efficiencies for all gamma lines of interest.

NMIJ/AIST calibrated the peak count efficiencies for Cs-134 and Cs-137 using standard solutions filled in the same type of containers as that of the sample containers. The volume of the solution was approximately the same as that of the sample. The difference of the peak count efficiencies and self-absorptions between the solution and the sample were adjusted by Monte-Carlo simulation.

BEV, JRC-Geel, SMU and TENMAK-NÜKEN used nuclear data from DDEP. CIEMAT, ENEA-INMRI, IFIN-HH, KRISS, NMISA, and NMIJ/AIST used those from Monographie BIPM-5, which was the same as those of DDEP. IJS used the Table of Radioactive Isotopes (1986). NIST did not use nuclear data in evaluating the peak count efficiencies.

8. Detector used

All participants used high purity germanium detector(s). The relative efficiencies of the detectors were 29 to 130 %. IJS, KRISS and NIST used analog signal processing, while other participants used digital signal processing. The characteristics of the detectors and signal processing are listed in Table 5. NMIJ/AIST used a high-purity germanium detector (ORTEC GEM 130-108, coaxial-type, 89.9 mm diameter, 76.2 mm long, p-type, 1.5 mm thick aluminum end cap). Signals from the detector were processed by a digital spectroscopy amplifier with triangle shaping and a multi-channel pulse height analyzer.

9. Measurement methods

All participants measured the activity of the sample using gamma ray spectrometry with high purity germanium detectors, whose code was UA-GH-GR-00-00-00 (see Appendix 2). Measurement methods used by the participants are summarized in Table 6.

Table 5. Detectors used by the participants.

Institute	Manufacturer, model	Shape, nature	Relative efficiency, crystal size [mm] FWHM	Entrance window	Radiation shield	Signal processing	Spectrometry software
BEV		p-type Coaxial	⌀56×54	Al, 2 mm		Inspector 2000	Genie 2000, LabSOCS, Geometry Composer
CIEMAT	Canberra Gx3520	Extended-range Coaxial, electrically cooled	35 % 1.1 keV (122 keV) 1.8 keV (1333 keV)				Genie 2000 GANAAS software
ENEA-INMRI	ORTEC GEM40-83-S	Coaxial p-type	40 % ⌀65.9×55.5			DSPEC	Gamma-Vision 5.2
IFIN-HH	ORTEC GEM25P4	Coaxial p-type	29 %, ⌀58.8×46 0.78 keV (121.78 keV) 1.73 keV (1332 keV)	Al, 1.27 mm	Pb 10 cm Cu 1mm Sn 1 mm	DSPEC PLUS	Gamma Vision-32 v.6.01
IJS (PB)	PGT	p-type	36 %	Al cap	Pb 16 cm (*1) Cd 1 mm Cu 2 mm	Analog signal Processing	Genie ESP, upgraded with additional home developed software
IJS (MG)	PGT	n-type	35 %	Mg cap	Pb 12 cm (*1) Cu 2 mm Paraffin 10 cm	Analog signal Processing	Genie ESP, upgraded with additional home developed software
IJS (BL)	ORTEC	Coaxial n-type	50 %	Be window	Pb 10 cm Hg 1 cm Cd 1 mm Cu 1.5 mm	Analog signal Processing	Genie ESP, upgraded with additional home developed software
IJS (SE)	ORTEC	n-type	40 %	Be window	Pb 10 cm Hg 1 cm Cd 1 mm Cu 1.5 mm	Analog signal Processing	Genie ESP, upgraded with additional home developed software
IJS (HG)	Canberra	Planar p-type	50 %	Be window	Pb 10 cm (*1) Hg 1 cm Cd 2 mm Cu 2 mm	Analog signal Processing	Genie ESP, upgraded with additional home developed software

Table 5. Detectors used by the participants (continued).

Institute	Manufacture, model	Shape, nature	Relative efficiency, crystal size [mm] FWHM	Entrance window	Radiation shield	Signal processing	Spectrometry software
JRC-Geel (CAN3)	Canberra	Coaxial p-type	90 %	Al, 1.0 mm	Pb 5 cm (*2) Pb 10 cm	Lynx MCA	Genie 2000
JRC-Geel (Ge-6)	Canberra	Coaxial p-type	80 %	Cu, 1.0 mm	Pb 5 cm (*2) Pb 5 cm	Lynx MCA	Genie 2000
JRC-Geel (Ge-3, in HADES)	Eurisys	Coaxial p-type	60 %	Al, 0.7 mm	Electrolytic Cu 14 cm Pb 14 cm (*2)	Lynx MCA	Genie 2000
KRISS (HPGe(A))		p-type	73.3 % ⌀69.0×98.9			Analog signal processing	
KRISS (HPGe(B))		p-type	71 % ⌀69.0×88.3			Digital signal processing	
NIST	Canberra GR7023	Reverse electrode Coaxial	⌀74.5×66.5		Pb 9 - 10 cm Cu ~ 1.5 - 2 mm Cd ~ 1 mm Steel ~ 1 cm	Canberra 2025 ORTEC 927 ASPEC MCA	MAESTRO
NMISA	Canberra GC3018	Coaxial p-type	32.2 % ⌀62.10×40.10 1.64 keV (1333 keV)		Pb 10 cm (*2) Cu 1.6 mm Sn 1 mm	Lynx DSP	Genie2000
SMU	Canberra GC3020	Coaxial p-type	30 % 2.0 keV (1333 keV)			DSA2000	Genie 2000
TENMAK-NÜKEN	PGT IGC 50195	Coaxial p-type	58.5 % 1.94 keV (1333 keV)	Al 1.5 mm		DSA1000	Genie 2000 Colegram software (LNHB)
NMIJ /AIST	ORTEC GEM 130-108	Coaxial p-type	130 % ⌀89.9×76.2	Al 1.5 mm	Pb 11 cm Cu 5 mm Acrylic 15 mm	MCA-7 (Seiko EG&G)	DSP-300 (Seiko EG&G)

(*1) The shield used was lead produced in the 1950s. (*2) The shield used was low-background lead.

Table 6. Measurement methods.

Institute	Container	Number of measurements	Measurement time	Typical peak count			Area calculation	Mean date of measurement
				605 keV	796 keV	662 keV		
BEV (*1)	⌀64×11 mm	2 samples, twice	12 000 s to 72 800 s	2200	2900	18500	non-linear squares fit, weighted mean	30 Jun. 2018
CIEMAT	U-8 (*2)	3 samples, 4 times	200 000 s	+	+	+		15 Jul. 2018
ENEA-INMRI	100 cm^3	1 sample, once	500 000 s	5498	4671	54858	weighted mean	8 Nov. 2018
IFIN-HH	U-8 (*2)	3 samples	15 000 s to 28 800 s	105 to 293	Not used	1359 to 2603	ROI of 3 FWHM	16 May 2018
IJS (*3)	⌀90 mm	3 samples, 5 detectors	~ 1 day	+	+	+	peak areas calculated using 3 independent peak area determination algorithms, each line averaged and weighted mean of 4 lines	11 Aug. 2018
JRC-Geel	radon-free Teflon	3 samples, 3 detectors Detector – sample gaps CAN3: 10 mm, directly on endcap Ge-3: 2.2 mm, 15 mm Ge-6: 15 mm, directly on endcap	950 000 to 2 500 000	12355 to 24364	9126 to 17500	119305 to 235692	3 dependent algorithms, weighted mean	17 Aug. 2018
KRISS	U-8 (*2)	3 samples, 2 detectors	200 000 s to 250 000 s	+	+	+	weighted mean	25 Jun. 2018
NIST	⌀83×40 mm	3 replicates, 3 times Detector – sample gap 5 mm	86 000 s to 521 000 s	+	+	+	three methods used equal statistical weight	24 Oct. 2018

Table 6. Measurement methods (continued).

Institute	Container	Number of measurements	Measurement time	Typical peak count			Area calculation	Mean date of measurement
				605 keV	796 keV	662 keV		
NMISA (*4)	75 cm^3	3 samples, 3 times	2×6 h 1×20 h	436 -20 h	275 -20 h	4200 -20 h	weighted mean of 3 lines of each measurement and arithmetic mean of 9 measurements	19 Aug. 2018
SMU	Marinelli beaker 450 cm^3	1 sample, 6 times	3×6 0000 s 2×240 000 s 1×600 000 s	+	+	+	weighted mean	2 Nov. 2018
TENMAK-NÜKEN (*5)	⌀6×5 cm	3 samples, once	510 000 s to 580 000 s	+	+	+	weighted mean	11 Oct. 2018
NMIJ/AIST	U-8 (*2)	3 samples, once	80 000 s	Not used	+	+	Covel method	8 Jul. 2015 (*6)

(*1) BEV also used other peaks: 475, 563, 569, 802, 1168 and 1365 keV.

(*2) U-8 is a type of sample container distributed by NMIJ/AIST.

(*3) IJS also used other peaks of 563 and 569 keV.

(*4) NMISA also used a peak of 802 keV.

(*5) TENMAK-NÜKEN also used a peak of 569 keV.

(*6) NMIJ/AIST measured the sample activity during sample preparation.

Table 7. Adjustment applied to the measurement (+: considered in participant's measurement, blank: not mentioned).

Institute	Background measurement	Coincidence summing	Self-absorption	Decay to reference date	Decay during measurement	Water content	Live time	Geometry	Remarks
BEV	8 spectra, 200000 s	+	LabSOCS						
CIEMAT [13]		PENNUC	PENNUC						
ENEA-INMRI	Measured container without sample	+	+	+	+	+			
IFIN-HH	Measured with a blank volume sample, 28800 s	GESPECOR V4.2	+	+	neglected	+	+	+	
IJS	Compensated	+	+			+ (*1)			+ (*1)
JRC-Geel		+	+		+			+	
KRISS			+						
NIST	no peak	+	+		+	+			
NMISA	Compensated, 87 h spectrum	+	+	+	+	+	+		
SMU	0.00372 s^{-1} subtracted from Cs-137			+					
TENMAK-NÜKEN	no peak	+	+		+				
NMIJ/AIST		+	+		+	+			

(*1) At first, IJS reported its results per mass of sample received (wet mass), but corrected its results subsequently (dry mass).

10. Moisture content

BEV, ENEA-INMRI, IFIN-HH, KRISS, NIST, NMISA, SMU and NMIJ/AIST estimated the water content in 3 g wheat flour samples by drying the sample in an oven at 135±3 °C for 1 h, according to the technical protocol of this comparison (CCRI(II)-S13) [14].

CIEMAT estimated the water content according to the same technical protocol, but also estimated it by drying the sample in an oven at 105 °C for 3 h. There was a difference of approximately 1.1 % in the moisture determination by both methods.

IJS dried 4 g of sample at 135 °C for 24 h.

JRC-Geel estimated the water content according to both the technical protocol of this comparison and the Karl-Fischer titration method. The relative uncertainties were given by the maximum of the relative difference between those obtained by the two techniques (1.4 %).

TENMAK-NÜKEN estimated the water content according to the technical protocol of this comparison, but also estimated it using an Ohaus automatic moisture content analyzer. The results for all the participants are given in Table 8.

Table 8. Flour content, moisture content and standard uncertainty.

Institute	Sample No.	Flour content $\frac{dry\ mass}{wet\ mass}$	Moisture content $\frac{wet\ mass - dry\ mass}{wet\ mass}$	Standard uncertainty
BEV	1	0.8837 (=1/1.131639)	0.1163	0.0042
	2	0.8833 (=1/1.132123)	0.1167	0.0042
	3	0.8817 (=1/1.134181)	0.1183	0.0042
CIEMAT	---	0.8867	0.1133	0.0056 (=0.0063*0.8867)
ENEA-INMRI	---	0.8814	0.1186	0.0006 (=0.00068*0.8814)
IFIN-HH	22	0.8824	0.1176	0.0003
	23	0.8897	0.1103	0.0003
	24	0.8909	0.1091	0.0003
IJS	37	0.903	0.097	0.004
	38	0.896	0.104	0.004
	39	0.900	0.100	0.004
JRC-Geel (*1)	4	0.8826	0.1174	0.0002
	5	0.8820	0.1180	0.0002
	7	0.8821	0.1179	0.0002
JRC-Geel (*2)	4	0.8810	0.1190	0.00125
	5	0.8808	0.1192	0.00125
	7	0.8828	0.1172	0.0012

Table 8. Flour content, moisture content and standard uncertainty (continued).

Institute	Sample No.	Flour content $\frac{dry\ mass}{wet\ mass}$	Moisture content $\frac{wet\ mass - dry\ mass}{wet\ mass}$	Standard uncertainty
KRISS	17	0.9014	0.0986	0.0015
	19	0.9011	0.0989	0.0025
	20	0.9005	0.0995	0.0010
	Average	0.9010	0.0990	0.0061
NIST	---	0.8782	0.1218	0.0003
NMISA	46	0.8850	0.1150	0.0007
SMU	---	0.87909	0.12091	0.00056
TENMAK-NÜKEN (*3)	---	0.8845	0.1155	0.0003
TENMAK-NÜKEN (*4)	---	0.8853	0.1147	0.0009
NMIJ/AIST	---	0.8781	0.1219	0.0036

(*1) according to the CCRI(II)-S13 technical protocol [14].
(*2) by the Karl-Fischer titration method.
(*3) according to the CCRI(II)-S13 technical protocol [14].
(*4) using an Ohaus automatic moisture content analyzer.

11. Results

BEV used peaks of 475 keV, 563 keV, 569 keV, 605 keV, 796 keV, 802 keV, 1168 keV and 1365 keV for Cs-134. CIEMAT, ENEA-INMRI, JRC-Geel, KRISS, NIST and SMU used peaks of 605 keV and 796 keV. IFIN-HH used the peak of 605 keV. IJS used the peaks of 563 keV, 569 keV, 605 keV and 796 keV. NMISA used the peaks of 569 keV, 605 keV, 796 keV and 802 keV. TENMAK-NÜKEN used the peaks of 569 keV, 605 keV and 796 keV. NMIJ/ASIT used the 796 keV peak.

The reference date was 1 March 2018, UTC 0:00:00. The half-lives of Cs-134 and Cs-137 used to estimate the activities at the reference date were 2.0644(14) years and 30.05(8) years, respectively [15-16]. IJS used 754.28(22) days for the half- life of Cs-134 and 30.17(16) years for that of Cs-137. The difference in the results due to the difference of the half-life was less than 0.1 %; therefore, no adjustment was applied to the IJS results.

The laboratory final results and their standard uncertainties are summarized in Table 9 for Cs-134 and Table 10 for Cs-137. Figures 1 and 2 show the final laboratory results with their standard uncertainties. Typical pulse height spectra, those of JRC-Geel and NIST, are introduced in Figures 3 to 5. The calculation of the SCRVs and their associated uncertainties for Cs-134 and Cs-137 were performed using the PMM [7], following the decision of CCRI(II) in its meeting of May 2013. The PMM [7] of the laboratory final results for Cs-134 was 10.99 Bq kg^{-1} and the standard uncertainty was 0.22 Bq kg^{-1} at the reference date. The PMM for Cs-137 was 96.5 Bq kg^{-1} and the standard uncertainty was 1.0 Bq kg^{-1}. The uncertainty budgets of each participant are listed in Table 11 for Cs-134 and Table 12 for Cs-137. The results of all participants were used to calculate the PMMs. IJS also determined the activity of K-40 as (50.5±1.5) Bq kg^{-1}.

Table 9. Final results and standard uncertainties for Cs-134.

Institute	Final result / (Bq kg^{-1})	Standard uncertainty / (Bq kg^{-1})	Relative standard uncertainty / %
BEV	9.5	0.5	5.3
CIEMAT	11.21	0.76	6.81
ENEA-INMRI	10.76	0.25	2.3
IFIN-HH	9.6	0.9	9.4
IJS	11.3	0.3	3.0
JRC-Geel	11.41	0.26	2.3
KRISS	11.61	0.25	2.14
NIST	11.2	0.3	2.9
NMISA	9.3	0.8	8.7
SMU	11.05	0.25	2.3
TENMAK-NÜKEN	11.40	0.26	2.28
NMIJ/AIST	11.6	0.3	2.3
Power-moderated mean	10.99	0.22	---

Table 10. Final results and standard uncertainties for Cs-137.

Institute	Final result / (Bq kg^{-1})	Standard uncertainty / (Bq kg^{-1})	Relative standard uncertainty / %
BEV	99	4	4.0
CIEMAT	92.66	2.02	2.18
ENEA-INMRI	93.9	1.8	1.9
IFIN-HH	100.0	3.5	3.5
IJS	99.3	3.0	3.0
JRC-Geel	99.7	2.2	2.2
KRISS	95.71	1.04	1.09
NIST	93.0	2.0	2.1
NMISA	85.7	5.9	6.9
SMU	97.2	2.7	2.8
TENMAK-NÜKEN	97.3	1.8	1.83
NMIJ/AIST	101.0	2.1	2.1
Power-moderated mean	96.5	1.0	---

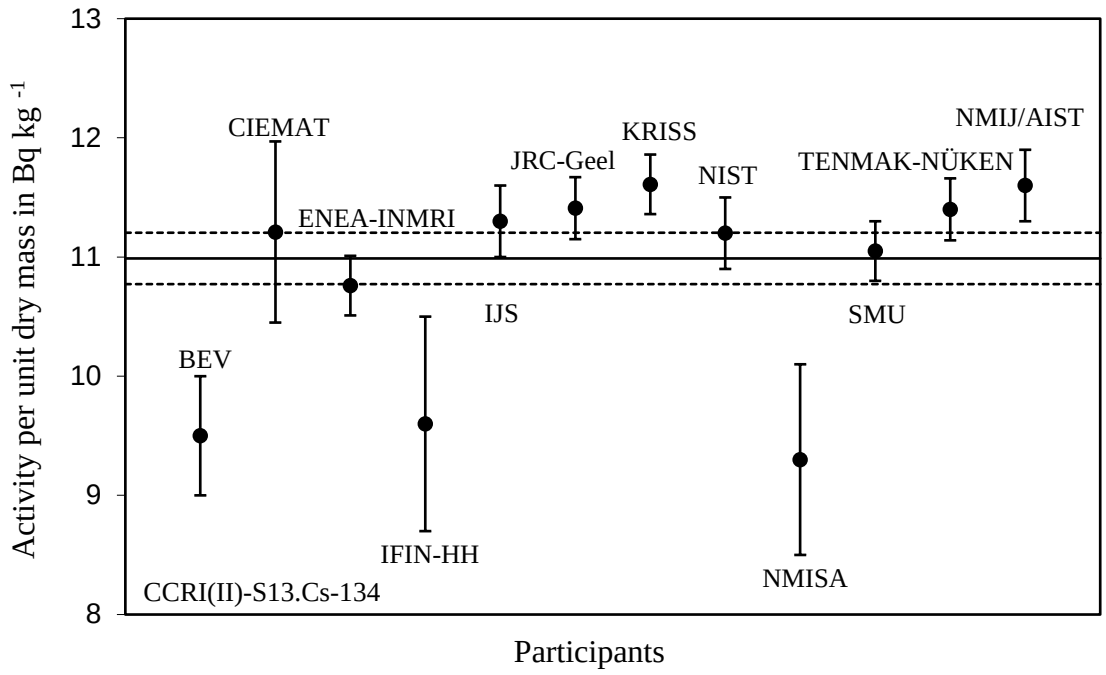

Figure 1. The laboratory final results for Cs-134 with their standard uncertainties listed in Table 9. The solid horizontal line indicates the PMM [7] of the final results of all participants. The dashed horizontal lines indicate the associated standard uncertainty.

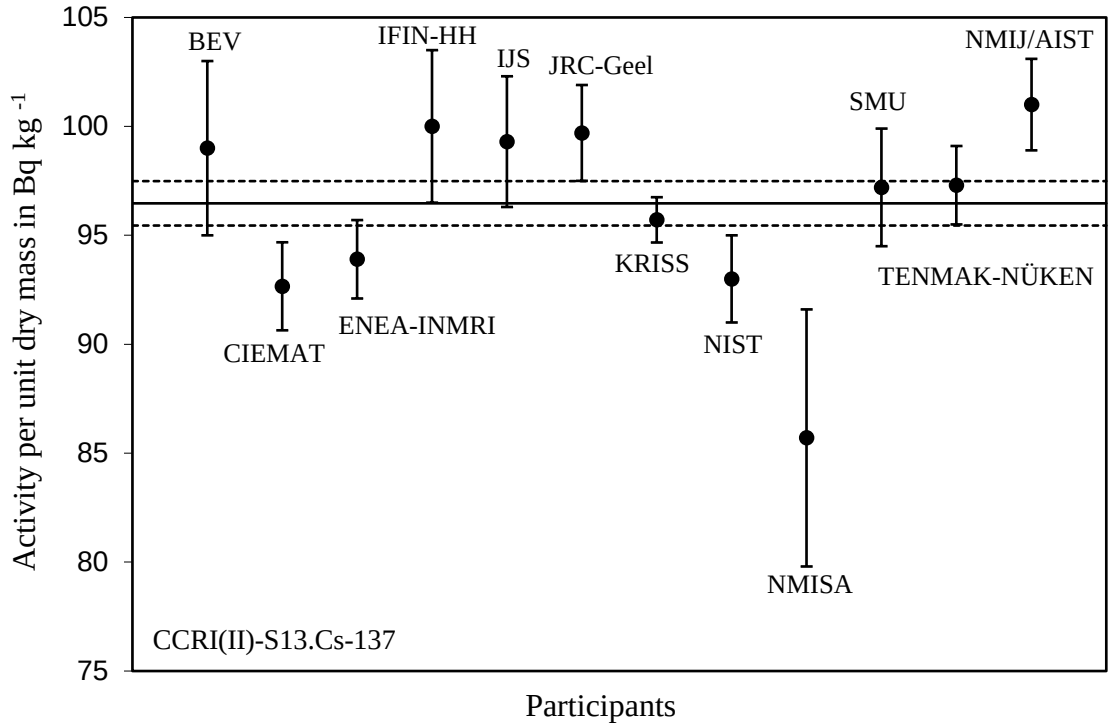

Figure 2. The laboratory final results for Cs-137 with their standard uncertainties listed in Table 10. The solid horizontal line indicates the PMM [7] of the final results of all participants. The dashed horizontal lines indicate the associated standard uncertainty.

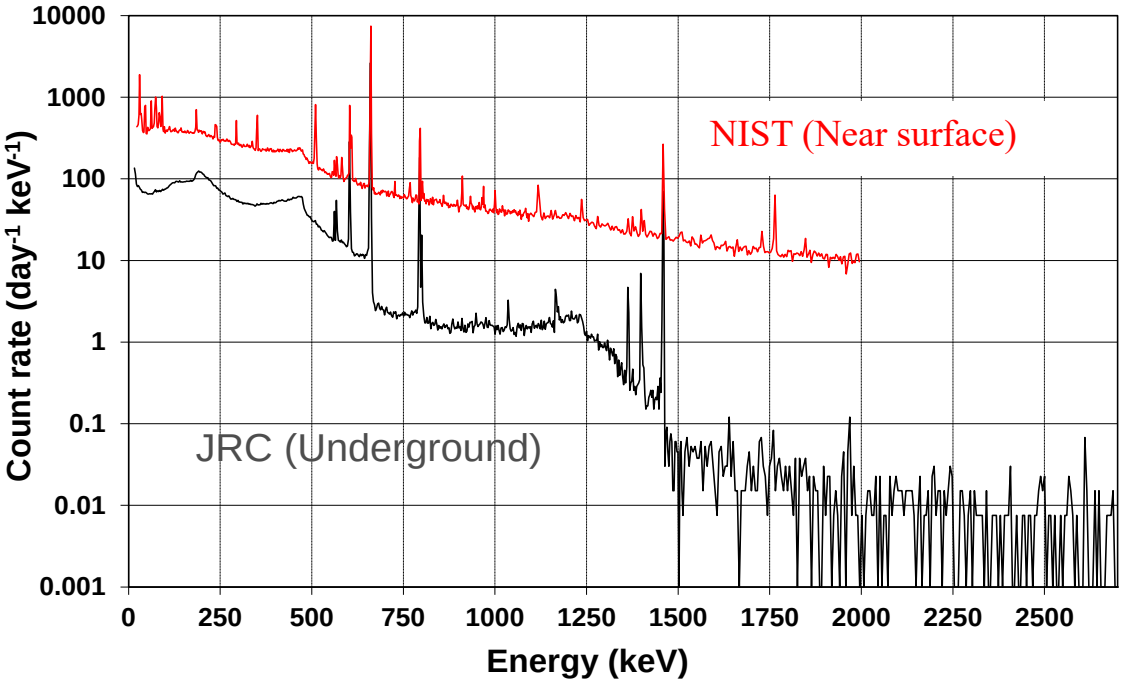

Figure 3. Spectra from measurements of wheat sample No. 33 near surface (in the basement) at NIST (70 g sample for 2.7 days) and wheat samples No. 7 (JRC-Geel) in the underground laboratory HADES (53.7 g sample for 24.2 days). At NIST the sample was placed 5 mm above the endcap of a coaxial reversed electrode HPGe-detector with height and diameter of 74.5 mm and 66.5 mm, respectively. At HADES the sample was placed 2.21 mm above the endcap of a coaxial HPGe-detector with height and diameter of 75.4 mm and 66 mm, respectively.

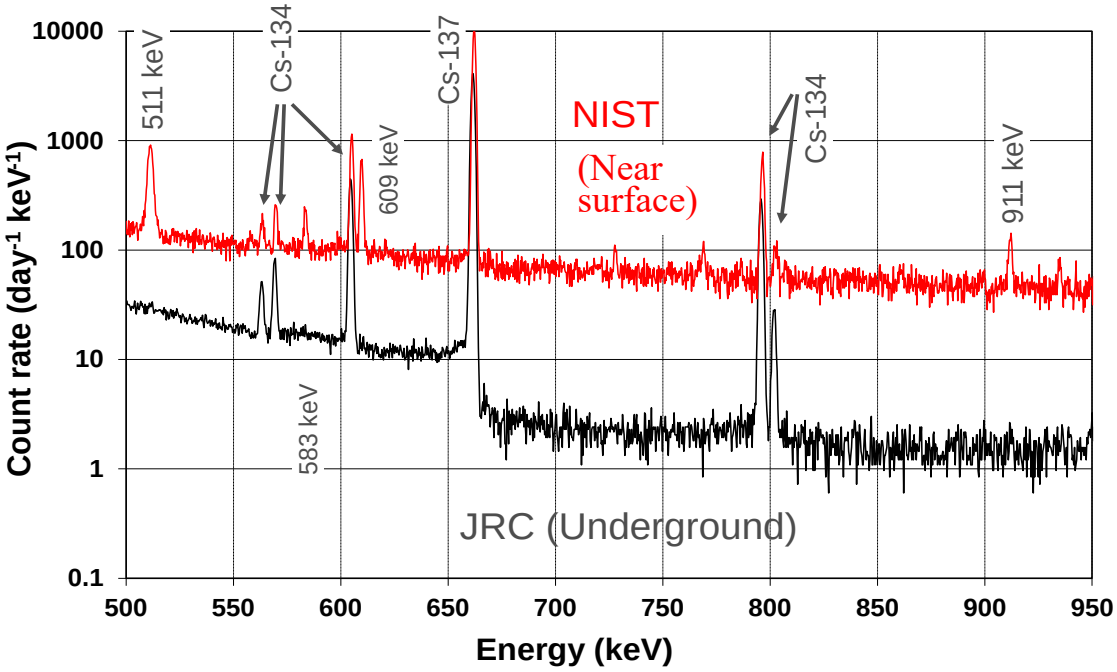

Figure 4. Same data as in Figure 3, but a zoom on the energy interval 500-950 keV with the main gamma-lines from Cs-134 and Cs-137. Background lines are identified with their respective energy; 511 keV (annihilation), 583 keV (Tl-208), 609 keV (Bi-214), 911 keV (Ac-228).

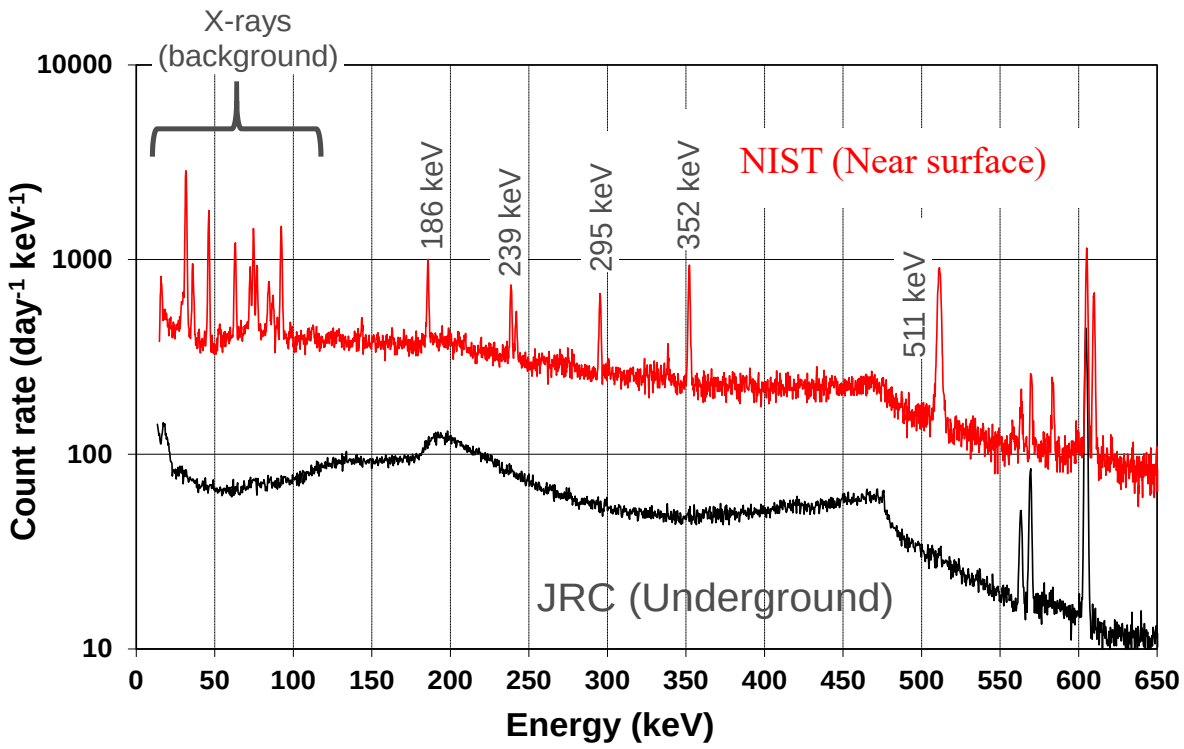

Figure 5. Same data as in Figure 4, but a zoom on the energy interval 0-650 keV. Background lines are identified with their respective energy; 186 keV (Ra-226), 239 keV (Pb-212), 295 keV and 352 keV (Pb-214), 511 keV (annihilation).

Notes: The continuum count rate of JRC-Geel was roughly one tenth of that of NIST in the energy region with the three main peaks of Cs-134 and Cs-137 as shown in Figure 4. The NIST and JRC-Geel detectors are almost identical in size and shape. At NIST the sample was 5 mm way from the detector and at JRC-Geel 2.2 mm, The fact that the sample at NIST had more mass and a bigger diameter compensates for the extra 2.8 mm distance from endcap. Therefore, the FEP efficiencies of the two detectors are relatively equal. The main cause of the difference was that the measurement system of JRC-Geel was installed in the underground laboratory HADES. Muons create neutrons by interacting with lead, which activate copper used as shield material; in HADES (225 meters below ground), the muons were shielded. Therefore, a copper shield whose thickness was up-to 10-15 cm was used. Furthermore, JRC-Geel used radiopure materials for building the detector and its front-end electronics. The inner volume of the shield was continuously purged by nitrogen gas supplied from the liquid nitrogen coolant. [17]

NIST's measuring system is located in a basement room with a high ceiling whose height from the floor was ~ 4.9 m. The ceiling was 0.3 m or more of concrete. The walls of the room consisted of ~ 0.6 m of low-potassium concrete. The measuring system was not equipped with an anti-coincidence or Compton suppression system. It did not have an air-purging system. (Jerome La Rosa, personal communication, 17 March 2023)

Table 11. Uncertainty components and estimated relative values / 10^{-2} (Cs-134).

Item No.	Function	BEV	CIEMAT	ENEA-INMRI 605 keV	ENEA-INMRI 796 keV	IFIN-HH (*1)
1	Counting statistics	4.0	6.51			8.1
1-1	Counting statistics (sample)			1.92	2.41	
1-2	Counting statistics (blank)			0.92	0.25	
2	Calibration factor	3.0	1	2.00	2.0	4.9
3	Decay correction to reference date	0.02	< 0.01	0.012	0.012	0.0044
3-1	Decay correction during measurement			0.054	0.054	
4	Live time correction	0.01	< 0.01			0.011
4-1	Live time correction (sample)			0.10	0.10	
4-2	Live time correction (blank)			0.00092	0.00025	
5	Sample configuration reproducibility	1.5		N.A.	N.A.	included in #2
6	Sample-calibration source geometry difference	0	1.1	N.A.	N.A.	included in #2
7	Sample-calibration source self-absorption difference	0	included in #2	0.24	0.50	included in #2
8	Instrument stability	0.7	< 0.01	0.60	0.60	N.A.
9	Weighing	0.3	0.1	0.20	0.20	1.23
10	Moisture content estimation	0.5	0.63	0.068	0.068	0.03
11	Homogeneity			0.95	0.95	
12	Compensation of sum coincidence	0.3	1.1	0.29	0.17	1
13	Photon emission probability		0.1	0.082	0.10	0.08
14	Others	0				
Combined standard uncertainty		5.3	6.81	3.2	3.4	9.6

(*1) The values of IFIN-HH are those obtained for one of three samples.

Table 11. Uncertainty components and estimated relative values / 10^{-2} (Cs-134) (continued).

Item No.	Function	IJS (*2)	JRC-Geel	KRISS	NIST
1	Counting statistics	2.7	< 1	2.03	2
1-1	Counting statistics (sample)				
1-2	Counting statistics (blank)				
2	Calibration factor	2.3	1.3	0.65	1.5
3	Decay correction to reference date	-	< 0.1	0.01	0.1
3-1	Decay correction during measurement			0.00	
4	Live time correction	0.0004	< 0.1	N.A.	negligible
4-1	Live time correction (sample)				
4-2	Live time correction (blank)				
5	Sample configuration reproducibility	included in #2	< 0.1	N.A.	1
6	Sample-calibration source geometry difference	N.A.	< 0.1	N.A.	1
7	Sample-calibration source self-absorption difference	N.A.	0.2	0.08	< 0.1
8	Instrument stability	-	< 0.1	0.10	< 0.1
9	Weighing	0.001	< 0.1	0.10	0.1
10	Moisture content estimation	0.004	1.4	0.06	0.25
11	Homogeneity	1			
12	Compensation of sum coincidence	-	0.5	N.A.	0 (*3)
13	Photon emission probability		< 0.1	0.09	
14	Others				
Combined standard uncertainty		3.7	2.3	2.14	2.9

(*2) The IJS mentioned that the uncertainty components marked with "-" were not taken into account in evaluating the combined standard uncertainty.

(*3) Calibrated by the source whose geometry was the same as that of the sample.

Table 11. Uncertainty components and estimated relative values / 10^{-2} (Cs-134) (continued).

Item No.	Function	NMISA	SMU (*4)	TENMAK-NÜKEN	NMIJ /AIST
1	Counting statistics	2.4	0.64	1.00	1.14
1-1	Counting statistics (sample)				
1-2	Counting statistics (blank)				
2	Calibration factor	-	2.3	1.73	1.56
3	Decay correction to reference date	0.01	0.012	0.15	0.05
3-1	Decay correction during measurement				
4	Live time correction	0.01	0.02	-	< 0.01
4-1	Live time correction (sample)				
4-2	Live time correction (blank)				
5	Sample configuration reproducibility	2.9	0.05	negligible	< 0.01
6	Sample-calibration source geometry difference	6.0	0.05	0.5	0.59
7	Sample-calibration source self-absorption difference	included in #6	0.1	-	0.10
8	Instrument stability	0.6	0.1	negligible	0.55
9	Weighing	0.06	0.01	0.15	< 0.01
10	Moisture content estimation	0.07	0.46	-	0.39
11	Homogeneity			0.95	
12	Compensation of sum coincidence	5.0	0.5	negligible	- (*5)
13	Photon emission probability				
14	Others: Measuring time				0.10
14-1	Background count				0.08
14-2	Difference between samples				0.75
Combined standard uncertainty		8.7	2.5	2.28	2.26

(*4) The values of SMU are those obtained for one individual measurement.

(*5) Calibrated by the source whose geometry was the same as that of the sample.

Table 12. Uncertainty components and estimated relative values / 10^{-2} (Cs-137).

Item No.	Function	BEV	CIEMAT	ENEA-INMRI	IFIN-HH (*1)
1	Counting statistics	3.0	1.44		2.1
1-1	Counting statistics (sample)			0.47	
1-2	Counting statistics (blank)			0.089	
2	Calibration factor	2.0	1	1.6	2.7
3	Decay correction to reference date	0.02	< 0.01	0.0042	0.0012
3-1	Decay correction during measurement			0.27	
4	Live time correction	0.01	< 0.01		0.011
4-1	Live time correction (sample)			0.10	
4-2	Live time correction (blank)			0.00043	
5	Sample configuration reproducibility	1.5		N.A.	Included in #2
6	Sample-calibration source geometry difference	0	1.1	N.A.	included in #2
7	Sample-calibration source self-absorption difference	0	included in #2	0.31	included in #2
8	Instrument stability	0.7	<0.01	0.60	N.A.
9	Weighing	0.3	0.1	0.20	1.23
10	Moisture content estimation	0.5	0.63	0.068	0.03
11	Homogeneity			0.27	
12	Compensation of sum coincidence				
13	Photon emission probability		0.24	0.24	0.24
14	Others	0			
Combined standard uncertainty		4.0	2.18	1.9	3.6

(*1) The values of IFIN-HH are those obtained for one of three samples.

Table 12. Uncertainty components and estimated relative values / 10^{-2} (Cs-137) (continued).

Item No.	Function	IJS (*2)	JRC-Geel	KRISS	NIST
1	Counting statistics	0.8	< 1	0.64	0.5
1-1	Counting statistics (sample)				
1-2	Counting statistics (blank)				
2	Calibration factor	2.7	1.3	0.83	1.5
3	Decay correction to reference date	0.0008	< 0.1	0.00	0.1
3-1	Decay correction during measurement			0.00	
4	Live time correction	-	< 0.1	N.A.	negligible
4-1	Live time correction (sample)				
4-2	Live time correction (blank)				
5	Sample configuration reproducibility	included in #2	< 0.1	N.A.	1
6	Sample-calibration source geometry difference	N.A.	< 0.1	N.A.	1
7	Sample-calibration source self-absorption difference	N.A.	0.2	0.08	< 0.1
8	Instrument stability	-	< 0.1	0.10	< 0.1
9	Weighing	0.001	< 0.1	0.10	0.1
10	Moisture content estimation	0.004	1.4	0.06	0.25
11	Homogeneity	1			
12	Compensation of sum coincidence				
13	Photon emission probability		< 0.1	0.24	
14	Others				
Combined standard uncertainty		3.0	2.2	1.09	2.1

(*2) The IJS mentioned that the uncertainty components marked with "-" were not taken into account in evaluating the combined standard uncertainty.

Table 12. Uncertainty components and estimated relative values / 10^{-2} (Cs-137) (continued).

Item No.	Function	NMISA	SMU (*3)	TENMAK-NÜKEN	NMIJ /AIST
1	Counting statistics	1.4	0.16	0.40	0.48
1-1	Counting statistics (sample)				
1-2	Counting statistics (blank)				
2	Calibration factor	-	2.8	1.68	1.81
3	Decay correction to reference date	0.003	0.0086	0.05	0.01
3-1	Decay correction during measurement				
4	Live time correction	0.01	0.02	included in #3	< 0.01
4-1	Live time correction (sample)				
4-2	Live time correction (blank)				
5	Sample configuration reproducibility	2.9	0.1	negligible	< 0.01
6	Sample-calibration source geometry difference	6.0	0.05	0.5	0.82
7	Sample-calibration source self-absorption difference	included in #6	0.1	included in #6	0.10
8	Instrument stability	0.6	0.1	negligible	0.24
9	Weighing	0.06	0.01	0.15	< 0.01
10	Moisture content estimation	0.07	0.46	included in #9	0.39
11	Homogeneity			0.27	
12	Compensation of sum coincidence			negligible	
13	Photon emission probability				
14	Others: Measuring time				0.10
14-1	Background count				0.03
14-2	Difference between samples				0.02
Combined standard uncertainty		6.9	2.9	1.83	2.10

(*3) The values of SMU are those obtained for one individual measurement.

12. Degrees of equivalence

The degree of the equivalence (DoE) from the result of a particular NMI *i* with the SCRV is expressed as the difference D_i between the values:

$$D_i = x_i - x_{ref}, \quad (3)$$

where x_i and x_{ref} are each result from the participants and the SCRV obtained by the PMM [7], respectively. The expanded uncertainty (k = 2) of this difference U_i, is known as the equivalence uncertainty; therefore:

$$U_i = 2u(D_i). \quad (4)$$

When the result of the NMI *i* is included in the SCRV with weighting of w_i, then:

$$u^2(D_i) = (1-2w_i)\, u_i^2 + u^2(x_{ref}), \quad (5)$$

where u_i is the combined standard uncertainties as reported by each laboratory. However, when the result of the NMI *i* is not included in the SCRV, then

$$u^2(D_i) = u_i^2 + u^2(x_{ref}). \quad (6)$$

The criteria of coverage factor for including in the SCRV calculation is 2.5 in this international comparison. The weighting w_i obtained by the PMM calculation is listed in Table 13. The preliminary degrees of equivalence for each participant in the comparison are presented in Table 14 for Cs-134 and Table 15 for Cs-137.

Table 13. Weighting w_i obtained by the PMM calculation.

Institute	Cs-134	Cs-137
BEV	0.07338	0.04851
CIEMAT	0.05064	0.09694
ENEA-INMRI	0.10052	0.10479
IFIN-HH	0.04180	0.05722
IJS	0.09525	0.06808
JRC-Geel	0.09949	0.09086
KRISS	0.10052	0.13303
NIST	0.09525	0.09764
NMISA	0.04790	0.02815
SMU	0.10052	0.07580
TENMAK-NÜKEN	0.09949	0.10479
NMIJ/AIST	0.09525	0.09420

Table 14. Degrees of equivalence (Cs-134).

Institute	Difference, D_i (Bq kg^{-1})	Expanded uncertainty (k=2) of the difference, U_{Di} (Bq kg^{-1})
BEV	-1.49	1.02
CIEMAT	0.22	1.50
ENEA-INMRI	-0.23	0.62
IFIN-HH	-1.39	1.78
IJS	0.31	0.69
JRC-Geel	0.42	0.63
KRISS	0.62	0.62
NIST	0.21	0.69
NMISA	-1.69	1.58
SMU	0.06	0.62
TENMAK-NÜKEN	0.41	0.63
NMIJ/AIST	0.61	0.69

Table 15. Degrees of equivalence (Cs-137).

Institute	Difference, D_i (Bq kg^{-1})	Expanded uncertainty (k=2) of the difference, U_{Di} (Bq kg^{-1})
BEV	2.53	7.87
CIEMAT	-3.81	4.16
ENEA-INMRI	-2.57	3.79
IFIN-HH	3.53	6.90
IJS	2.83	5.94
JRC-Geel	3.23	4.47
KRISS	-0.76	2.71
NIST	-3.47	4.13
NMISA	-10.77	11.64
SMU	0.73	5.38
TENMAK-NÜKEN	0.83	3.79
NMIJ/AIST	4.53	4.30

13. Conclusion

The CCRI(II) supplementary comparison of measurement of an activity per unit mass of Cs-134 and Cs-137 in wheat flour (CCRI(II)-S13) was successfully completed. Twelve institutes reported their results. The SCRV for Cs-134 at the reference date of 1 March 2018 UTC 0:00:00 was 10.99 Bq kg^{-1} and its standard uncertainty was 0.22 Bq kg^{-1} based on the power-moderated mean [7]. That for Cs-137 was 96.5 Bq kg^{-1} and its standard uncertainty was 1.0 Bq kg^{-1}.

Acknowledgements

The authors would like to thank the CCRI/KCWG(II) and BIPM staff for their continuous support. They also would like to appreciate Dr. Mikael Hult of JRC-Geel and Dr. Jerome La Rosa of NIST for preparing the Figures 3 - 5 based on the reported spectra and for supplying additional information concerning their measurement systems. Finally, they would like to express their special thanks to Dr. Lisa Karam, a chair of CCRI(II), for encouraging and giving many helpful suggestions.

References

[1] T. Miura, A. Yunoki, Y. Unno, S. Hamamatsu, M. Hachinohe and S. Todoriki, The Development of SI Traceable Brown Rice Certified Reference Material for Caesium 134 and Caesium 137 Measurement, RADIOISOTOPES (in Japanese), Vol. 65, No. 4, 157-167 (2016).

[2] M. Hachinohe, S. Todoriki, Y. Unno, T. Miura, A. Yunoki and S. Hamamatsu, Preparation of Certified Reference Materials for Radioactivity Measurement Using Brown Rice, RADIOISOTOPES (in Japanese), Vol. 65, No. 4, 169-180 (2016).

[3] Y. Unno, M. Hachinohe, S. Hamamatsu, S. Todoriki, A. Yunoki and T. Miura, Characterization of brown rice as a certified reference material for Fukushima accident-related radioactivity measurements, Appl. Radiat. Isot. 87 (2014) 485-488.

[4] Y. Unno, A. Yunoki, T. Miura, S. Hamamatsu, M. Hachinohe and S. Todoriki, Proficiency Test of Radioactivity Measurement Using Samples of Brown Rice, RADIOISOTOPES (in Japanese), Vol. 65, No. 4, 181-190 (2016).

[5] A. Yunoki, et. al., APMP supplementary international comparison of activity measurement of Cs-134 and Cs-137 in brown rice (APMP.RI(II)-S3.Cs-134.Cs-137), *Metrologia*, 2023, 60, *Tech*. *Suppl*., 06007.

[6] JCGM, *Evaluation of measurement data – Guide to the expression of uncertainty in measurement*, JCGM 100:2008.

[7] S. Pommé and J Keightley, Determination of a reference value and its uncertainty through a power-moderated mean, *Metrologia* 52 (2015) S200-S212.

[8] R. Furukawa, Y. Unno, T. Miura, A. Yunoki, M. Hachinohe, S. Hamamatsu, Homogeneity of wheat flour in 5 ml containers for certified reference materials, Appl. Radiat. Isot. 134 (2018) 32-34.

[9] T. Yamada and Y. Nakamura, Examination of the U8 type polypropylene container used for radioactivity standard volume source, RADIOISOTOPES (in Japanese), Vol. 54, 105-110 (2005).

[10] ISO Guide 35: 2017 Reference materials – General and statistical principles for certification, International Organization for Standardization, Geneva.

[11] G. Lutter, M. Hult, G. Marissens, H. Stroh, F. Tzika, A gamma-ray spectrometry analysis software environment, Appl. Radiat. Isot., 134 (2018), pp. 200-204.
[12] S. Kaminski, A. Jakobi, Chr. Wilhelm, Uncertainty of gamma-ray spectrometry measurement of environmental samples due to uncertainties in matrix composition, density and sample geometry, Appl. Radiat. Isot., 94 (2014), pp. 306-313.
[13] García-Toraño, E., Peyrés, V., Bé, M.M., Lépy, M.-C., Dulieu, C., V., Salvat, F., 2017. Simulation of decay processes and radiation transport times in radioactivity measurements, Nucl. Instrum. Methods B 396, 43–49.
[14] Technical protocol CCRI(II) supplementary international comparison - Measurement of an activity per unit mass of Cs-134 and Cs-137 in wheat flour -, https://www.bipm.org/kcdb/comparison?id=655.
[15] M. –M. Be *et al.*, Monographie BIPM-5, 2013, **Vol. 7** – A = 14 to 245, 73-79.
[16] M. –M. Be *et al.*, Monographie BIPM-5, 2006, **Vol. 3** – A = 3 to 244, 91-98.
[17] M.Hult, G. Lutter, G. Marissens and H. Stroh, JRC Serving policy and science at the HADES underground research facility–- a casebook, EUR 30207 EN, Publications Office of the European Union, Luxembourg, (2020), ISBN 978-92-76-18589-5, doi:10.2760/056079, https://publications.jrc.ec.europa.eu/repository/handle/JRC120311.

Appendix 1 Acronyms used to identify different measurement methods.

Each acronym has six components, geometry-detector (1)-radiation (1)-detector (2)-radiation (2)-mode. When a component is unknown, ?? is used and when it is not applicable 00 is used.

Geometry	**acronym**	**Detector**	**acronym**
4π	4P	proportional counter	PC
defined solid angle	SA	press. prop counter	PP
2π	2P	liquid scintillation counting	LS
undefined solid angle	UA	NaI(Tl)	NA
		Ge(HP)	GH
		Ge-Li	GL
		Si-Li	SL
		CsI	CS
		ionization chamber	IC
		grid ionization chamber	GC
		bolometer	BO
		calorimeter	CA
		PIPS detector	PS
Radiation	**acronym**	**Mode**	**acronym**
positron	PO	efficiency tracing	ET
beta particle	BP	internal gas counting	IG
Auger electron	AE	CIEMAT/NIST	CN
conversion electron	CE	sum counting	SC
Bremsstrahlung	BS	coincidence	CO
gamma ray	GR	anti-coincidence	AC
X – rays	XR	coincidence counting with efficiency tracing	CT
alpha - particle	AP	anti-coincidence counting with efficiency tracing	AT
mixture of various radiation e.g. X and gamma	MX	triple-to-double coincidence ratio counting	TD
		selective sampling	SS

Examples method	**acronym**
4π(PC)β–γ-coincidence counting	4P-PC-BP-NA-GR-CO
4π(PPC)β–γ-coincidence counting efficiency tracing	4P-PP-MX-NA-GR-CT
defined solid angle α-particle counting with a PIPS detector	SA-PS-AP-00-00-00
4π(PPC)AX-γ(GeHP)-anticoincidence counting	4P-PP-MX-GH-GR-AC
4π CsI-β,AX,γ counting	4P-CS-MX-00-00-00
calibrated IC	4P-IC-GR-00-00-00
internal gas counting	4P-PC-BP-00-00-IG